POAC'23
Glasgow, United Kingdom

Proceedings of the 27th International Conference on
Port and Ocean Engineering under Arctic Conditions
12-16 June 2023, Glasgow, United Kingdom

FREE PROPULSION AND MANOEUVRING TESTS OF THE KOREAN ICEBREAKER *ARAON* IN ICE

Michael Lau[1], Seong-Rak Cho[2], Ayhan Akinturk[1]
[1]National Research Council of Canada, Ocean, Coastal and River Engineering, St. John's, NL, Canada
[2]Korea Research Institute of Ships and Ocean Engineering, Daejeon, Korea

ABSTRACT

The National Research Council of Canada's Ocean, Coastal and River Engineering Research Centre (NRC), with the support of the Korea Research Institute of Ships and Ocean Engineering (KRISO), has conducted a series of propulsion and free manoeuvring tests on a scale model of the Korean icebreaker *ARAON*. Investigation of the podded propulsors and their influence on ice-hull load distribution were conducted in open water, level ice, and pack ice. With control over propeller shaft speed and pod deflection angle the tests included straight, zigzagging, and turning arc runs. Throughout testing, the model's position, pod performance characteristics, and ice-hull pressures were monitored. A relationship between RPS and pod angle setting and model motion was determined, level ice turning and zigzag channel measurements were taken, and pressure distribution observations were made. Significant ice-hull loading was experienced over the model's bow and outside stern during turning arcs, while high loading was experienced at the bow during straight-going runs. Relatively low ice-hull loading was observed at the model's stern during straight-going runs. Comparison between loading on inside and outside turning surfaces was made. These observations from the *ARAON* were also compared with datasets obtained elsewhere.

KEY WORDS: Propulsion, Manoeuvring; Ice; *ARAON*; Model test

INTROCTION

Podded propellers have become widely accepted in the marine industry over the past decade due to their superior manoeuvrability over the conventional screw-driven systems particularly in ice-covered waters. This rapid adoption has outpaced the understanding of ship manoeuvring performance with such drives. Specifically, the higher turning rate with podded propulsion results in a very different load profile and pressure distribution on the hull compared to conventional propulsion (Lau, 2021a & 2021b). This technology gap may result in unsafe operations and severe ship loading conditions, as most personnel training, ship design and marine regulation paradigms are dated prior to the emergence of podded propulsion.

The Korean new icebreaker *ARAON* is equipped with twin pod propulsion units. Its owner, the Korea Research Institute of Ships and Ocean Engineering (KRISO), completed its first 2 sets

of *ARAON* sea trials in January 2010 (Likhomanov, 2010) and July to August 2010 (Lee et al., 2014); while, the National Research Council of Canada's Ocean, Coastal and River Engineering Research Centre (NRC), with the support of KRISO, conducted an extensive series of model tests of the *ARAON* in both free running and captive conditions in various ice conditions beyond the scope of the sea trials.

This paper describes the free propulsion and manoeuvring model tests of the *ARAON*, including details of the experiment and highlights of some results. The performance of the *ARAON* was also compared with datasets obtained elsewhere.

THE FACILITY, MODEL AND INSTRUMENTATION

The *ARAON* model tests were performed at the NRC's 96 meters long, 12 meters wide, and 3 meters deep ice tank in St. John's. For these tests, Correct Density EG/AD/S model ice was used (Spencer and Timco, 1990).

All experiments were carried out on a 1:20 scaled model of the *ARAON* (Model #850) shown in Figure 1. The model self-propels itself longitudinally down the tank with the carriage operator "chasing" it with the carriage. The model surface was finished to a friction coefficient of 0.05. The characteristics of the *ARAON* model are given in Table 1. The model is equipped with two azimuthing podded propulsors (see Figure 2). Table 2 summarizes the geometry of the propulsors in greater detail.

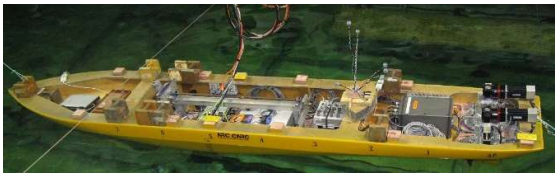

Figure 1. ARAON model in tank, with festoon, full ballast and instrumentation

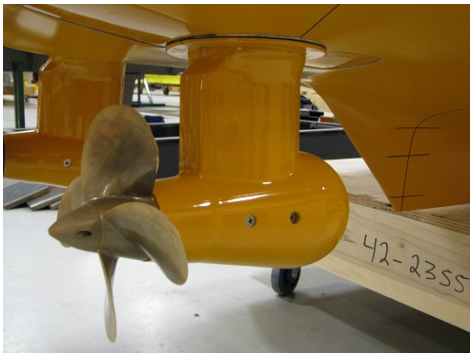

Figure 2. Starboard pod installed on the model

Table 1. Hydrostatics of *ARAON* model (Model #850)

Characteristic	**Model #850**	**Full Scale**
Length between Perpendiculars (m)	5.36	107.2
Beam Overall (m)	0.9513	19.026
Draft (m)	0.34	6.8
Center of Buoyancy Forward of Mid-Ship (m)	2.3303	46.606
Displacement (kg)	441.26	3530080

Table 2. Geometry of model propellers used on IOT Model #850 podded propulsors

Diameter, (model/full scale)	200 mm / 4 m
Number of blades	4
Hub-Diameter (H/D) ratio	0.26
Expanded area ratio, EAR	0.6
Pitch distribution	constant P/D=1.0
Hub taper angle	15°

The on-board instrumentation was powered by a cable festoon, which was connected to the carriage. There were 62 data channels recorded during the experiments capturing data from various load and motion sensors, including global pod forces and moments, propeller thrust and torque, ship motions and hull pressure.

The global pod dynamometer was attached to the strut of each pod to measure the forces and moments (six components) exerted on the ship by the pod units. Each pod was also equipped with a set of load cells to measure the thrust and torque on the propeller shaft.

The model motions, in six degrees of freedom, were measured by ADIS™ and MotionPak™. In parallel, the NRC's QualiSys™ motion capture system was also deployed to provide redundancy for the motion measurements.

Eight I-Scan® tactile pressure sensor panels were taped to the hull in various locations as shown in Figure 3 and Figure 4 shows the tactile pressure sensing panel. Table 3 gives the location of all sensors. The I-Scan® sensors, are matrix based with approximately 2,000 sensing elements with pressure registered as electrical resistance. The outputs were converted to contact force distribution and captured as color-coded video by Tekscan™ (Figure 5).

In addition, two video cameras, which were mounted on the carriage, and a handheld video camera were used to record the model behaviour during the tests. The fixed cameras showed the starboard side (profile) and bow (overhead) of the model. An underwater camera was also used for certain tests.

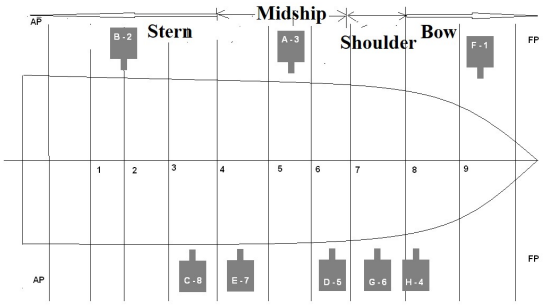

A

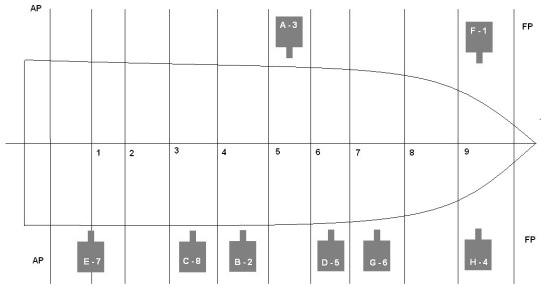

B

Figure 3. Pressure sensor arrangements in (A) open water runs and 20 mm ice runs and (B) 40 mm and 60 mm ice runs (vertical lines indicate the general location of model stations; ship profile not of scale; location of regions approximated)

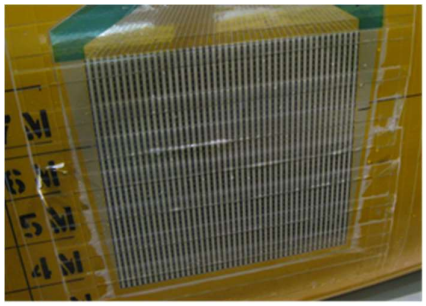

Figure 4. I-Scan® tactile pressure sensing panel

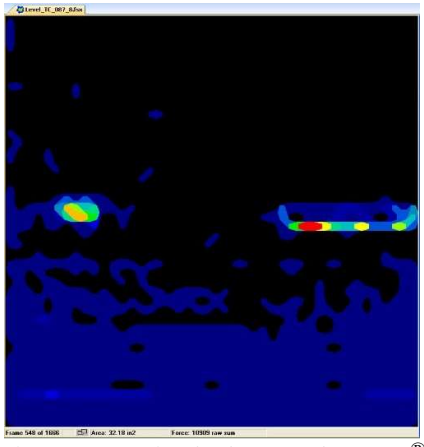

Figure 5. A single frame of I-Scan® pressure output in a Tekscan™ movie

Table 3. Pressure sensor locations

Sensor	Location (Distance from AP)	
	A (m)	B (m)
F-1	4.564	4.564
B-2	0.867	2.354
A-3	2.564	2.564
H-4	4.271	4.652
D-5	3.341	3.341
G-6	3.860	3.860
E-7	2.354	0.640
C-8	1.860	1.860

THE TEST PROGRAM

The test program consisted of straight, zigzagging and turning arcs runs in open water, level ice, and pack ice conditions. All turns were made to starboard, such that starboard was always the inside hull surface. The propeller speed was fixed for each run. Both static and dynamic azimuthing angles were used. The azimuthing rate of the pods was set to 20^o per second. Position, model and pod performance data and hull pressure were recorded.

The target thickness of the ice sheets ranged from 20, 40 to 60 mm, with a target flexural strength of 35 kPa (see Table 4). The crushing strength ranged from 51 to 61 kPa and the elastic modulus to flexural strength ratio ranged from 587 to 1655. A consistent set of tests was run in each test environment as summarized in Tables 5 and 6 for open water and ice tests, respectively. Further details of the test program can be found in Lau and Akinturk (2010).

Table 4. Summary of ice test conditions (full scale given in brackets)

Sheet	**Nominal Thickness (mm)**	**Measured Thickness (mm)**		**Target Strength (kPa)**	**Crushing Strength (kPa)**		E/σ_f
		North	**South**		**North**	**South**	
AZI1	20 (400)	20.9	20.4	35 (700)	44.8	58.1	587
AZI2	20 (400)	21.1	21.1	35 (700)	62.1	53.3	1358
AZI3	40 (800)	41.3	41.5	35 (700)	65.1	57.1	853
AZI4	60 (1200)	58.8	58.3	35 (700)	-	-	1655

Table 5. Test suite performed in open water

Test	Pod and Propeller Settings
Straight/Speed Runs	Tractor Mode/Forward, Tractor Mode/Reverse, Pusher Mode/Forward, Pusher Mode/Reverse; 0° azimuthing angle for both pods; Prop speeds up to 13.3 rps (59.5 rps full scale)
Turning Circle Manoeuvres	Tractor Mode/Forward; Various azimuthing pod angles from 0° to 360°; Prop speeds up to 13.3 rps
Zigzag Manoeuvres	Tractor Mode/Forward; Standard 10°/10° (prop speeds = 2.78, 8.1 & 10.7 rps) (12.4, 36.2 & 47.9 rps full scale); Standard 20°/20° (prop speeds = 8.1 rps)

Table 6. Test suite performed in ice

Test	Pod and Propeller Settings
Straight/Speed Runs	Tractor Mode/Forward; 0° azimuthing angle for both pods; Prop speeds = 8.1, 10.7, 13.3 & 16 rps (36.2, 47.9, 59.5 & 71.6 rps full scale)
Turning Circle Manoeuvres	Tractor Mode/Forward; 15°, 35° and 45° azimuthing angles for both pods; Prop speeds = 8.1, 10.7, 13.3 rps
Zigzag Manoeuvres	Tractor Mode/Forward; Standard 10°/10°; Prop speeds = 10.7 rps

TEST RESULTS

This paper highlights the trends observed in the ice-hull load distributions. For a more comprehensive analysis of test results, including pod performances and ship motions, we refer the reader to Lau and Akinturk (2010).

Speed Runs (Open Water)

Straight-going speed runs were completed in open water in order to provide a relationship between the propeller speed and the speed of the model. Positive propeller speed settings were used when the pods were in tractor mode (propellers forward of pod unit), whereas for pusher mode (propellers aft of pod units), the propeller speeds were negative.

Additional runs were performed with the model moving astern. In this case, negative propeller speed settings were used when the pods were in tractor mode, whereas for pusher mode, the propeller speeds were positive. The results are summarized in Figure 6.

In comparing the attained forwarding speed, Figure 6 suggests that the pod is about 10% more efficient when operating in the tractor mode. There is no apparent difference in efficiency between the two modes of operation when the model going backwards.

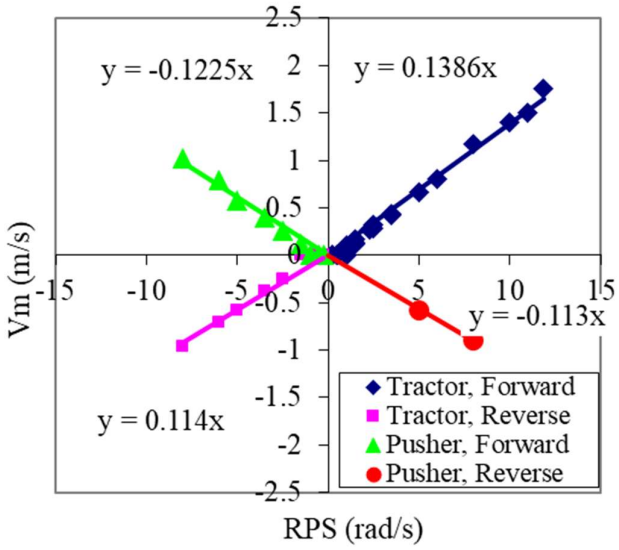

Figure 6. Results of open-water speed calibration runs

Pressure Distribution (in Level Ice)

The load distribution for each run is given in Figures 7 to 17 with the runs grouped according to test type and ice thickness. For the sensor locations/data point locations, please refer to Figure 3 and Table 3. The results are given in model scale, which can be scaled up to full scale values by a factor of 8000.

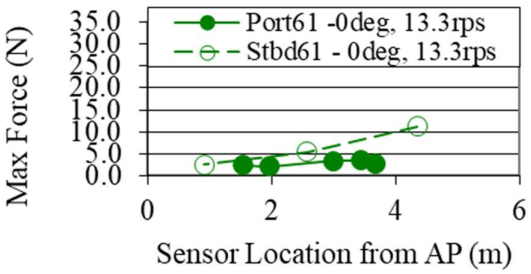

Figure 7. Ice-hull load distribution for straight run, 0° pod angle, 13.3 rps propeller speed and 20 mm ice

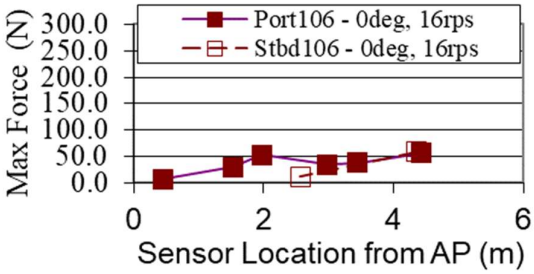

Figure 9. Ice-hull load distribution for straight run, 0° pod angle, 16.0 rps propeller speed and 60 mm ice

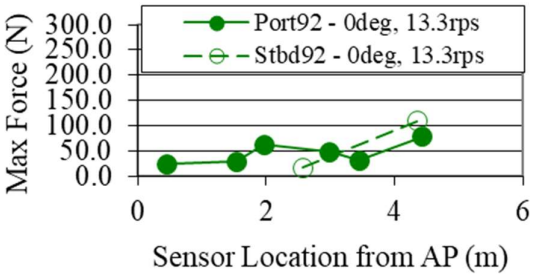

Figure 8. Ice-hull load distribution for straight run, 0° pod angle, 13.3 rps propeller speed and 40 mm ice

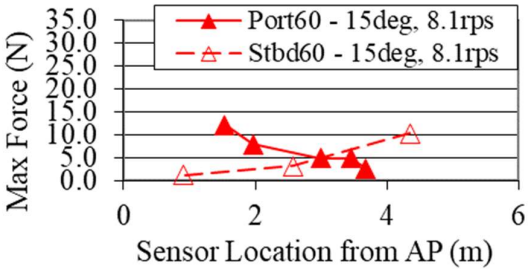

Figure 10. Ice-hull load distribution for turning circle, 15° pod angle, 8.1 rps propeller speed and 20 mm ice

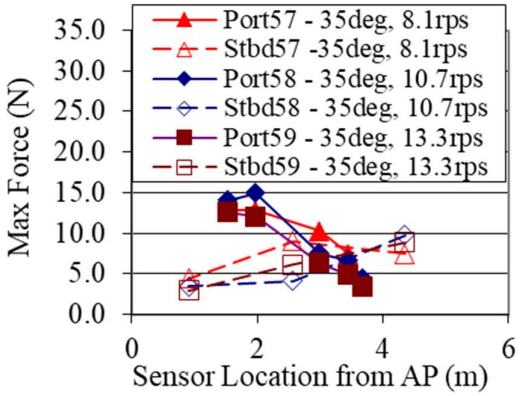

Figure 11. Ice-hull load distribution for turning circle, 35° pod angle, 8.1, 10.7 and 13.3 rps propeller speed and 20 mm ice

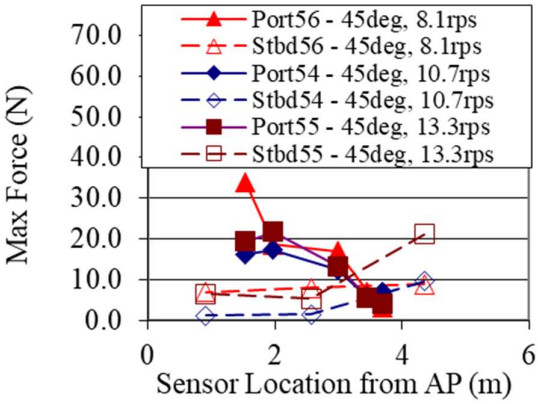

Figure 12. Ice-hull load distribution for turning circle, 45° pod angle, 8.1, 10.7 and 13.3 rps propeller speed and 20 mm ice

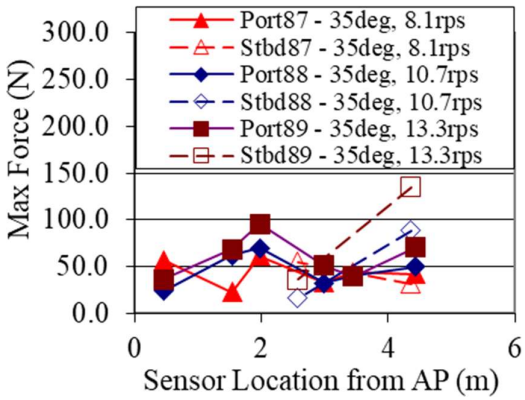

Figure 13. Ice-hull load distribution for turning circle, 35° pod angle, 8.1, 10.7 and 13.3 rps propeller speed and 40 mm ice

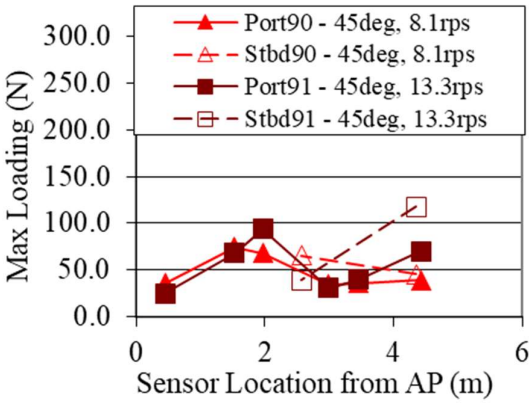

Figure 14. Ice-hull load distribution for turning circle, 45° pod angle, 8.1, 10.7 and 13.3 rps propeller speed and 40 mm ice

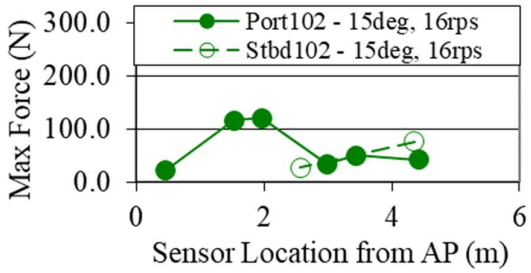

Figure 15. Ice-hull load distribution for turning circle, 15° pod angle, 16.0 rps propeller speed and 60 mm ice

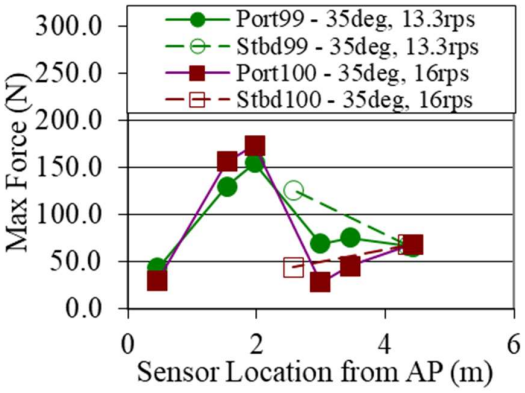

Figure 16. Ice-hull load distribution for turning circle, 35° pod angle, 13.3 and 16.0 rps propeller speed and 60 mm ice

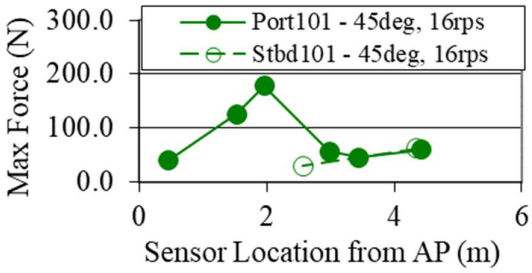

Figure 17. Ice-hull load distribution for turning circle, 45° pod angle, 16.0 rps propeller speed and 60 mm ice

Analysis of Pressure Data

For a preliminary analysis of the pressure data, the maximum loading given in Figures 7 to17 were averaged over all straight-going and turning circle tests, respectively, to show the data trends.

The average loading for each side of the hull during the turning arc tests is shown in Figure 18. The results show a similarity between loading at the bow at the inside and outside of the turn (approximately 48 N and 58 N, respectively), and relatively higher loading on the bow when compared with other hull regions, except the transition of the stern and midship at the outside hull surface. At this transition, significantly high loading (approximately 70 N) was observed at the outside hull surface, compared to almost non-existent loading on the inside stern. The shoulder hull surfaces at the outside of the turn show relatively moderate loading (approximately 29 N). Likewise, at mid-ship, the inside hull surface shows moderate loading, but there were no sensors mounted at the corresponding location on the outside hull surface (approximately 30 N).

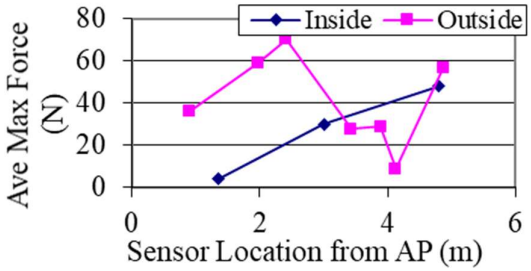

Figure 18. Ice-hull load distribution (inside and outside hull surfaces) in level ice turning arcs

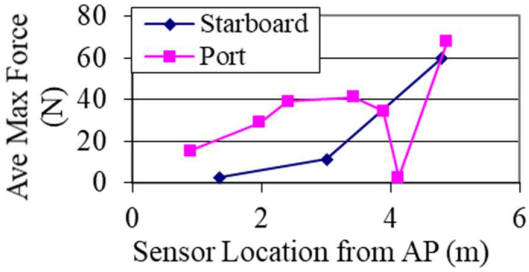

Figure 19. Ice-hull load distribution (port and starboard) in level ice straight runs

A similar comparison can be made for straight running tests. The average loading for each side is shown in Figure 19. As in the case of turning circle runs, the results show a similarity between loading at the starboard and port bow surfaces (approximately 60 N and 68 N, respectively), and the average of both bow sensors shows slightly higher loading when compared to other hull regions. High loading is evident at the outside shoulder hull surfaces, as well. At mid-ships, there is some difference in loading between the hull surfaces, however. The port surface appears to experience significantly higher loading. Since these were straight runs and thus one

would expect similar loading at both sides of the hull, this finding requires further investigation of the recorded data.

The stern exhibited lower loading than other regions as expected. At the stern, there is similarity between loading at the starboard and port hull surfaces, but with higher loading on the port.

The pressure distributions on the outside/port hull surface for turning circle tests are compared against the port side in the corresponding straight running tests. The average loading for each side is shown in Figure 20.

Some of the highest loading is observed over the two outside/port bow surface sensors in turning circles and straight-going tests, with both types of tests experiencing similar loading. The results show some of the highest loading over the two outside/port shoulder surface sensors in turning arcs and straight tests with slightly higher loading experienced during straight-going tests. Furthermore, the results show the highest loading (approximately 70 N) experienced at the outside/port mid-ship surface during turning, and mid-range loading (approximately 39 N) at the outside/port mid-ship surface during straight-going tests; whereas, the results show relatively low loading (approximately 18 N) at the outside/port stern hull surface during straight-going tests, and mid-range loading (approximately 38 N) at the outside/port mid-ship surface during turning circles.

Figure 21 shows the average loading for the inside/starboard hull surface during the turning arc tests in comparison with that for the starboard side during the straight runs. At the bow, the results show a similarity between loading in turning arc (approximately 48 N) and straight running (approximately 60 N) tests and considerably higher loading when compared with other hull regions. At mid-ships, the results show moderate loading at the inside/starboard hull surface during both straight runs and turning arcs (approximately 11 N and 30 N, respectively), with higher loading during turning arcs. Finally, the inside or starboard stern hull surface shows low loading during both straight runs and turning arcs (approximately 2 N and 4 N, respectively).

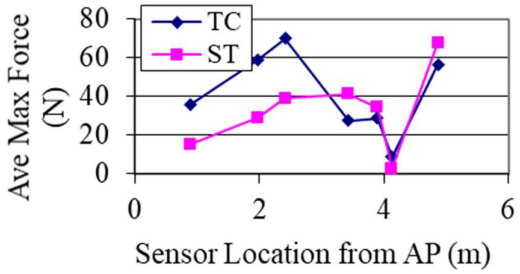

Figure 20. Ice-hull load distribution (outside/port) in level ice with straight runs and turning arcs

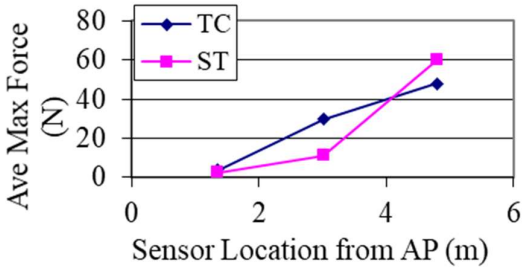

Figure 21. Ice-hull load distribution (inside/starboard) in level ice with straight runs and turning arcs

Observed Overall Trends

It is important to note that more definitive conclusions would be drawn from each test run, if an equal number of port- and starboard-mounted pressure sensors were used. With only three sensors mounted on the inside/starboard hull surface of the model, comparison between the inside and outside turning surfaces is difficult. Nevertheless, some preliminary observations can be made between the regions of the hull in different manoeuvres.

In the *ARAON* model turning circle tests, the highest loading was measured at the bow and the transition between mid-ship and stern. The findings here agree with the predictions of Su et al. (2009), Izumiyama (2007), Izumiyama et al. (2005), Harris (2006), and Matsuzawa et al. (2006). The fundamentals that can be extracted from these reports are that the bow must penetrate the ice and the stern will be forced to come in contact with the outer channel edge.

In the *ARAON* model straight-running tests, the highest loading was experienced at the bow/shoulder hull surfaces, while the lowest loading was experience at the stern.

Again, the findings here agree with the predictions of Izumiyama (2007), Izumiyama et al. (2005), Harris (2006), Takimoto et al. (2006) and Matsuzawa et al. (2006).

Matsuzawa et al. (2006) explain this low loading by noting that when the bow cuts a channel, it is slightly wider than the widest part of the model, and so the stern has little, if any, contact with the channel during straight-going runs.

The test results also show that the model experienced higher loading over the port side of the hull during straight-going tests. This is not consistent with any previous results, but may potentially be explained by the weight and subsequent manoeuvring influence of the festoon, an unbalance of instrumentation in the model, or sensor error. However, it must be acknowledged that this discrepancy could be caused by mismatched pod performance characteristics, or directional instability of the model (vessel) itself.

CONCLUSION

In this paper, a series of physical model tests of ship propulsion and manoeuvring characteristics in open water and ice is presented. It was part of a larger effort to investigate the performance of podded propulsors, as well as their potential influence on ice-hull load distribution patterns during ship manoeuvring. Some of the findings on load distribution are highlighted. A relationship between RPS and model motion was determined and pressure distribution observations were made. Significant ice-hull loading was experienced over the model's bow and outside stern during turning arcs, while high loading was experienced at the bow during straight-going runs. Very low ice-hull loading was observed at the model's stern during straight-going runs. Comparison between loading on inside and outside turning surfaces was limited, as a lower number of sensors were mounted on the model's inside turning surface. It is expected that the physical results from the *ARAON* model tests will better define the performance of the ship's design and capabilities. The results from these model tests will also serve as a standard comparison tool when refining and implementing any simulation model.

ACKNOWLEDGEMENTS

The authors wish to sincerely thank the Korea Research Institute of Ships and Ocean Engineering for their financial support under project "Development of ice performance test and evaluation technology for icebreaking ships (PES4700). Special thanks are also due to the technical personnel of the National Research Council of Canada's Ocean, Coastal and River Engineering Research Centre for their contributions to the model tests.

REFERENCES

Harris, T., 2006. *SAFEICE – Clearing a Path Through Icy Waters*. Helsinki University of Technology Ship Laboratory, Espoo, Finland.

Izumiyama, K., Wako, D., Shimoda, H. & Uto, S., 2005. Ice load measurement on a model ship hull. *Proceedings of the 18th International Conference on Port and Ocean Engineering Under Arctic Conditions*, Vol. 2, Potsdam, New York, pp. 635-646.

Izumiyama, K., 2007. Ice loads – model scale testing. SAFEICE Public Seminar, Kotka, Finland.

Lau, M., 2021a. OSIS-IHI simulation of the maneuvering performance of USCGC Mackinaw (WLBB-30). Part II: the simulation. *Proceedings of the 31st International Ocean and Polar Engineering Conference*, Rhodes, Greece.

Lau, M., 2021b. Effects of hull geometry and tightness of turns on ship maneuverability: an OSIS-IHI simulation. *Proceedings of the 40th International Conference on Offshore Mechanics and Arctic Engineering*, Virtual Conference.

Lau, M. & Akinturk, A., 2010. *Free Propulsion and Manoeuvring Test of the Korean Icebreaker ARAON In Ice*. OCRE-LM-2010-10, The National Research Council Canada's Ocean, Coastal and River Engineering Research Centre, St. John's, NL.

Lee, T.K., Lee, J.H., Kim, H.S. & Rim, C.W., 2014. Field measurement of local ice pressures on the *ARAON* in the Beaufort Sea. *International Journal of Naval Architecture and Ocean Engineering*, 6(4): 788-799.

Likhomanov, V., 2010. *Full-scale Ice Trials uf the Korean Research Icebreaker ARAON*. Russian Antarctic Expedition Report, Arctic and Antarctic Research Institute, Saint Petersburg, Russia.

Matsuzawa, T., Wako, D. & Izumiyama K., 2006. Local ice load on a ship with podded propulsors. *Proceedings of the 18th IAHR International Symposium on Ice*, Vol. 2, Sapporo, Japan, pp. 33-40.

Spencer, D. & Timco, G.W., 1990. CD model ice - a process to produce correct density (CD) model ice. *Proceedings of the 10th IAHR International Symposium on Ice*, Espoo, Finland, pp. 745-755.

Su, B., Riska, K. & Moan, T., 2009. A numerical method for the prediction of ship performance in level ice. *Cold Regions Science and Technology*, 60(3): pp. 177-188.

Takimoto, T., Uto, S., Oka, S., Murakami, C. & Izumiyama, K., 2006. Measurement of ice load exerted on the hull of icebreaker Soya in the Southern Sea of Okhotsk. *Proceedings of the 18th IAHR International Symposium on Ice*, Vol. 2, Sapporo, Japan, pp. 41-48.